Mon. Not. R. Astron. Soc. **382,** 840–848 (2007) doi:10.1111/j.1365-2966.2007.12416.x

Electron-impact rotational and hyperfine excitation of HCN, HNC, DCN and DNC

Alexandre Faure,[1⋆] Hemal N. Varambhia,[2] Thierry Stoecklin[3] and Jonathan Tennyson[2]

[1]*Laboratoire d'Astrophysique, UMR 5571 CNRS, Université Joseph-Fourier, BP 53, 38041 Grenoble Cedex 09, France*
[2]*Department of Physics and Astronomy, University College London, Gower Street, London WC1E 6BT*
[3]*Institut des Sciences Moléculaires, UMR 5255 CNRS, 351 cours de la Libération, 33405 Talence Cedex, France*

Accepted 2007 September 3. Received 2007 August 24; in original form 2007 August 1

ABSTRACT

Rotational excitation of isotopologues of HCN and HNC by thermal electron-impact is studied using the molecular R-matrix method combined with the adiabatic-nuclei-rotation approximation. Rate coefficients are obtained for electron temperatures in the range 5–6000 K and for transitions among all levels up to $J = 8$. Hyperfine rates are also derived using the infinite-order-sudden scaling method. It is shown that the dominant rotational transitions are dipole-allowed, that is, those for which $\Delta J = 1$. The hyperfine propensity rule $\Delta J = \Delta F$ is found to be stronger than that in the case of He–HCN collisions. For dipole-allowed transitions, electron-impact rates are shown to exceed those for excitation of HCN by He atoms by six orders of magnitude. As a result, the present rates should be included in any detailed population model of isotopologues of HCN and HNC in sources where the electron fraction is larger than 10^{-6}, for example, in interstellar shocks and comets.

Key words: molecular data – molecular processes – ISM: molecules.

1 INTRODUCTION

Hydrogen cyanide, HCN, and its isomer HNC are among the most abundant organic molecules in space, from star-forming regions to circumstellar envelopes and comets. HCN and HNC also belong to the small class of molecules detected in high-redshift galaxies, along with CO and HCO^+ (Guélin et al. 2007, and references therein). In addition to thermal emission from various rotational transitions within different vibrational states at (sub)millimetre and far-infrared wavelengths (see e.g. Cernicharo et al. 1996), a few masering lines have been detected towards several stars (e.g. Lucas & Cernicharo 1989). Numerous isotopologues have also been identified, in particular the deuterated species DCN and DNC (e.g Leurini et al. 2006, and references therein).

One interesting observation concerning rotational spectra of HCN is that of the 'hyperfine anomalies' (Walmsley, Churchwell & Fitzpatrick 1982, and references therein). At high resolution it is possible to resolve the hyperfine components arising from the nitrogen (^{14}N) nuclear spin for transitions arising from low-lying rotational levels. The hyperfine lines have been found in a number of cases (e.g. Izumiura, Ukita & Tsuji 1995; Park, Kim & Minh 1999; Ahrens et al. 2002, and references therein) to be not in thermal equilibrium with each other. These anomalies have been shown to depend on the degree of thermal overlap, on the opacity and on the collisional rates (e.g. Guilloteau & Baudry 1981; González-Alfonso & Cernicharo 1993; Turner 2001).

Already 30 yr ago, it was suggested that when the electron fraction exceeds $\sim 10^{-5}$, electron-impact excitation of polar molecules may be significant in addition to collisions with the most-abundant neutrals (Dickinson et al. 1977). Such conditions can be found, for example, in diffuse interstellar clouds and photon-dominated regions where $n(\mathrm{e})/n(\mathrm{H})$ can reach a few 10^{-4}. Recently, Lovell et al. (2004) devoted their study to the effect of electrons in the rotational excitation of cometary HCN. They showed that electron collisions are the dominant mechanism of HCN excitation in the comets Hale–Bopp and Hyakutake where the electron fraction, $n(\mathrm{e})/n(\mathrm{H_2O})$, lies in the range $\sim 10^{-5}$–1. The authors stated that accounting for electron collisions may thus alleviate the need for large HCN–H_2O cross-sections in models that neglect effects due to electrons. Similar conclusions were drawn in the case of water (Faure, Gorfinkiel & Tennyson 2004a, and references therein).

Recently, Jimenez-Serra et al. (2006) used rotational emissions of SiO, HCO^+, HCN and HNC to probe electron densities in C-type shocks. In particular, they ascribed differences in the ambient and precursor components to electron density enhancements during the first stages of the C-type shock evolution. The dipolar ion HCO^+ was found to be a sensitive tracer of this effect.

A theoretical determination of rotational cross-sections and rate coefficients for e–HCN was carried out by Saha et al. (1981) for the

⋆E-mail: afaure@obs.ujf-grenoble.fr

rotationally inelastic transitions $J = 0 \rightarrow 1$, J = 1 → 2 and $J = 0 \rightarrow 2$. Cross-sections were computed using the rotational close-coupling method and rate coefficients were obtained in the temperature range 5–100 K. An additional study includes that of Jain & Norcross (1985), where the adiabatic-nuclei-rotation (ANR) approximation was combined with model potentials. The cross-sections were computed for the same set of transitions as in Saha et al. (1981). In addition to electron scattering, the rotational excitation of HCN by He as a substitute for H_2 has been studied by Green & Thaddeus (1974), Green (unpublished data)[1] and Monteiro & Stutzki (1986) (see also references therein). The latter work also provided hyperfine rates for $J = 0$–4 and $T = 10$–30 K.

In this study, the molecular R-matrix method has been combined with the ANR approximation. We provide e–HCN rotational rates for transitions among all levels up to $J = 8$ and for temperatures in the range 5–6000 K. Hyperfine rates are obtained within the infinite-order-sudden (IOS) scaling method for $J = 0$–3. Comparisons to the previous theoretical studies and to differential data are also presented. In Section 2, R-matrix calculations are described and the procedure used to obtain rotational and hyperfine rates is briefly introduced. In Section 3, both cross-sections and rate coefficients are presented and discussed. Conclusions are given in Section 4.

2 CALCULATIONS

2.1 R-matrix calculation

Two of us (Varambhia & Tennyson 2007) have carried out R-matrix calculations on HCN and HNC at the close-coupling level in C_{2v} symmetry. The calculations were performed using the UK molecular polyatomic R-matrix package (Morgan, Tennyson & Gillan 1998) at the (fixed) equilibrium geometries of HCN and HNC using an R-matrix radius $10a_0$.

HCN and HNC (hence DCN and DNC) were represented by the 6-31G Gaussian type orbital (GTO) basis set. The target wavefunctions were computed using the complete active space configuration interaction (CASCI) method. They were subsequently improved using a pseudo-natural orbital calculation. The five lowest C_{2v} electronically excited states, $^1A_1$, $^3A_1$, $^3A_2$, $^3B_1$ and $^3B_2$, were employed and all possible single and double excitations to virtual orbitals were included. In order to incorporate the double excitation, however, it was necessary to freeze eight electrons (the 1s and 2s electrons of the C and N atoms). For both HCN and HNC, the weighting coefficients for the density matrix averaging procedure were 5.75, 1.5, 1.5, 1.5 and 1.5 for $^1A_1$, $^3A_1$, $^3A_2$, $^3B_1$ and $^3B_2$, respectively. This target model yielded dipole moments −2.87 D and −2.91 D for HCN and HNC, respectively, which can be compared to the experimental values −2.985 D (Ebenstein & Muenter 1984) and −3.05 D (Blackman et al. 1976).

The scattering wavefunctions were represented by a close-coupling expansion including 24 target electronic states, done to keep the expected shape resonance as low as possible. Calculations were performed on the scattering states $^2A_1$, $^2B_1$, $^2B_2$ and $^2A_2$. The continuum GTOs are those of Faure et al. (2002) and are expanded up to $g(l = 4)$ partial wave. One virtual orbital was allocated to each symmetry where target orbitals were available to do so. This scattering model also used the separable treatment of continuum and virtual orbitals in order to allow for increased polarizability and hence further reduce the position of any resonance yielded by the model. Further discussion on the problem of convergence of the polarization interaction in close-coupling methods can be found in Varambhia & Tennyson (2007), Gil et al. (1994) and Gorfinkiel & Tennyson (2004). The resulting fixed-nuclei (FN) (body-fixed) T-matrices were used to obtain the pure rotation excitation cross-section in the collision energy range 0.01–6.2 eV (see Section 3.2). The positions of the shape resonances for these molecules are inside the scattering energy ranges.

In the fixed-geometry approximation, the DCN and DNC electronic wavefunctions are identical to those of HCN and HNC, respectively. The distinction between the isotopologues therefore arises, in the present treatment, only from the different rotational excitation thresholds (see below).

2.2 Rotational cross-sections

We consider here an electron scattering from a polar linear neutral molecule in the FN approximation (Lane 1980). In this approach, the cross-sections are expressed as a partial-wave expansion within the ANR approximation which assumes that the initial and final target rotational states are degenerate. For low partial waves (here $l \leqslant 4$), the cross-section is computed from the FN T-matrices obtained via the R-matrix calculations. In the case of dipole forbidden transitions (i.e. those with $\Delta J > 1$), cross-sections are expected to converge rapidly and can be safely evaluated using FN T-matrices only (see Section 3.1). In the case of dipole allowed transitions ($\Delta J = 1$), however, the partial-wave expansion does not converge in the FN approximation, owing to the very long-range nature of the electron–dipole interaction. To circumvent this problem, the standard procedure is to use the dipolar Born approximation to obtain the cross-section for the high partial waves not included in the FN T-matrices (Crawford & Dalgarno 1971). In this case, the final cross-section is calculated as the sum of two contributions and can be regarded as a 'short-range correction' to the (dipolar) Born approximation.

The known unphysical behaviour of the FN cross-sections near rotational thresholds, inherent in the ANR approximation, is corrected using a simple kinematic ratio (Chang & Temkin 1970) which forces the excitation cross-sections to zero at threshold. In the case of e–H_2, this procedure has been shown to be accurate down to a collision energy $E \sim 2 \times \Delta E$ where ΔE is the rotational threshold (Morrison 1988). Recently, experimental data for the scattering of cold electrons with water have also confirmed the validity of the adiabatic 'threshold-corrected' approximation down to very low electron energies (Faure, Gorfinkiel & Tennyson 2004b; Čurík et al. 2006). Note that threshold effects could only be included rigorously in a full rotational close-coupling calculation, which is impractical at the collision energies investigated here. In this context, it is worth stressing that in the case of molecular ions, cross-sections are large and finite at threshold with a significant but moderate contribution from closed channels (Faure et al. 2006).

Finally, in order to make comparisons with available experimental data, differential cross-sections were computed using the Born-closure method for the scattering amplitude, as described in Itikawa (2000). In this approach, the high partial waves contribution ($l > 4$) due to the quadrupole and induced-dipole interactions was also included.

[1] The earlier calculations of Green & Thaddeus (1974) (restricted to the lowest eight levels of HCN and temperatures of 5–100 K) were extended in 1993 to obtain rate constants among the lowest 30 rotational levels and for temperatures of 100–1200 K. These unpublished results are available at http://data.giss.nasa.gov/mcrates/#hcn.

2.3 Hyperfine rates

The hyperfine interaction arises due to the very weak coupling of nuclear spin to the molecular rotation, which to an excellent approximation does not affect the overall collision dynamics. In the laboratory, Ahrens et al. (2002) measured ground-state rotational transitions of HCN using sub-Doppler saturation spectroscopy in the THz region. This technique enables features such as hyperfine structures to be revealed, which within Doppler limits, would remain hidden. Nine consecutive rotational transitions with their associated hyperfine structures have been thus partly resolved. Additional study includes that of Turner (2001). Here, the transitions $J = 1 \rightarrow 0$ and $2 \rightarrow 1$ were observed towards dark clouds for the deuterated molecules N_2D^+, DCN and DNC, from which molecular constants including the complex nuclear quadrupole hyperfine splitting were derived. More recently, the nuclear quadrupole hyperfine structure of HNC and DNC was resolved in the laboratory for the first time using millimetre-wave absorption spectroscopy (Bechtel, Steeves & Field 2006). New rest frequencies for the $J = 1 \rightarrow 0$, $J = 2 \rightarrow 1$ and $J = 3 \rightarrow 2$ rotational transitions of the ground vibrational state were determined. It was found that the hyperfine structure of HNC is dominated by the interaction of the valence shell electrons with the nuclear spin of the nitrogen atom. The hyperfine structure of DNC, however, was much more complicated due to the additional coupling of the deuterium nucleus ($I = 1$). This coupling gave rise to a septet in the $J = 1 \rightarrow 0$ transition.

As hyperfine structure is resolved in some of the astronomical spectra, it is crucial to know the rate coefficients among these energy levels. In the following, only the spin of the ^{14}N atom is considered as the effects of the spins of H and D atoms on the collisional rates are assumed negligible, although of course they affect the energy levels. Hyperfine states are labelled by J and F, where F is the total angular momentum obtained by coupling J to I, the nuclear spin ($I = 1$ for ^{14}N). If the hyperfine levels are assumed to be degenerate, it is possible to simplify considerably the hyperfine scattering problem (Corey & McCourt 1983). Within the ANR or IOS approximation, which both ignore the rotational spacings, the scattering equations are further simplified and the rates among rotational and hyperfine levels can be simply calculated in terms of 'fundamental' rotational rates, $k^{\rm IOS}$ ($L \rightarrow 0$):

$$k^{\rm IOS}(J \rightarrow J') = (2J'+1)\sum_L \begin{pmatrix} J & J' & L \\ 0 & 0 & 0 \end{pmatrix}^2 \times (2L+1)k^{\rm IOS}(L \rightarrow 0), \quad (1)$$

$$k^{\rm IOS}(JF \rightarrow J'F') = (2J+1)(2J'+1)(2F'+1) \times \sum_L \begin{pmatrix} J & J' & L \\ 0 & 0 & 0 \end{pmatrix}^2 \times \begin{Bmatrix} L & F & F' \\ I & J' & J \end{Bmatrix}^2 \times (2L+1)k^{\rm IOS}(L \rightarrow 0), \quad (2)$$

where

$$\begin{pmatrix} J & J' & L \\ 0 & 0 & 0 \end{pmatrix} \text{ and } \begin{Bmatrix} L & F & F' \\ I & J' & J \end{Bmatrix}$$

are Wigner-3j and Wigner-6j symbols, respectively.

However, as the ANR rotational cross-sections are corrected for threshold effects (see above), equations (1) and (2) are only moderately accurate for the actual rates. We have therefore implemented the 'scaling' method proposed by Neufeld & Green (1994) in which the hyperfine rates are obtained as a scaling of the rotational rates:

$$k(JF \rightarrow J'F') = \frac{k^{\rm IOS}(JF \rightarrow J'F')}{k^{\rm IOS}(J \rightarrow J')} k(J \rightarrow J'), \quad (3)$$

using the actual rates $k(L \rightarrow 0)$ for the IOS fundamental rates. For quasi-elastic transitions, that is, $JF \rightarrow JF'$ with $F \neq F'$, equation (2) is used directly, as recommended by Neufeld & Green (1994). Note that fundamental rates for *downward* transitions were employed as these were found to provide better results in the case of He–HCN for which accurate close-coupling hyperfine rates are available (Monteiro & Stutzki 1986).

Finally, it should be noted that within the IOS approximation, the allowed transitions or selection rules are determined by the Wigner-6j symbol, as expressed in equation (2). Interestingly, the same selection rules have been obtained by Chu (1976) and Varshalovich & Khersonskii (1977) from multipole expansion approaches. Radiative (dipolar) selection rules are also determined by the above 6j symbol with $L = 1$.

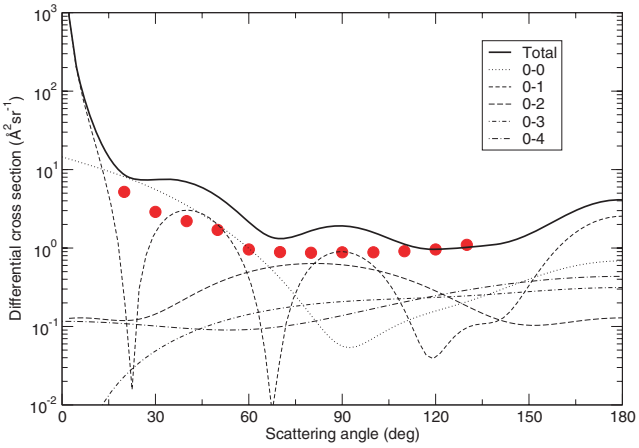

Figure 1. Differential cross-sections for vibrationally elastic scattering (rotationally summed) of electrons by HCN at 5 eV. Experimental data (full circles) are from Srivastava et al. (1978). The present calculation is given by the thick solid line. Other lines denote partial state-to-state differential cross-sections.

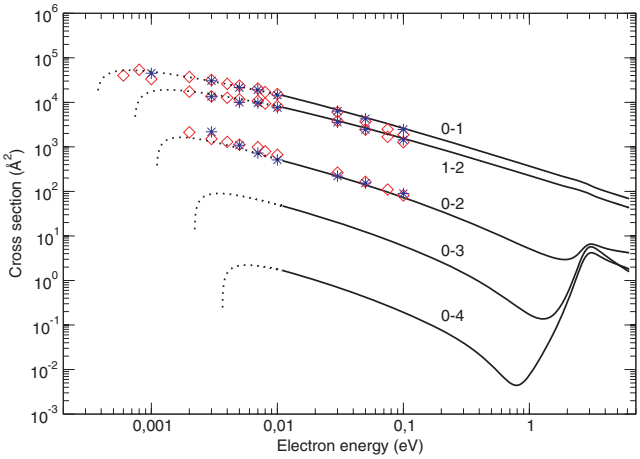

Figure 2. Integral cross-sections for rotationally inelastic scattering of electrons by HCN as a function of electron energy. The lozenges and stars denote the results of Saha et al. (1981) and Jain & Norcross (1985), respectively. The present calculations are given by the solid thick lines. The dotted lines are extrapolations (see the text).

3 RESULTS AND DISCUSSION

3.1 Cross-sections

The comparison with experimental differential cross-sections is often the only reliable way for testing electron–molecule calculations. In the case of polar targets, integral cross-sections deduced from experiments are indeed strongly dependent on the extrapolation procedure used to estimate the small-angle scattering which cannot be detected experimentally (e.g. Faure et al. 2004b).

We have computed the elastic (rotationally summed) differential cross-sections for electron scattering from HCN at the electron energy of 5 eV in order to compare our calculations with the experimental results of Srivastava et al. (1978). As shown in Fig. 1, our calculations reproduce the experimental data only qualitatively. Quantitatively, our results are larger by roughly a factor of 2 at angles $\theta \leqslant 100^\circ$. It can be noted that the dipolar transition $0 \rightarrow 1$ dominates over all other transitions at both forward and backward angles. Sharp dips are also observed in the $0 \rightarrow 1$ transition at about 20°, 70° and 120°. We note that these dips, which reflect rainbow scattering (e.g. Korsch & Ernesti 1992), are not completely suppressed by the contribution of the other transitions in the total curve. More experimental study is clearly necessary to interpret the difference between theory and experiment, as already suggested sometime ago by Jain & Norcross (1985).

Note that the Born completion was found to be crucial in the case of the dipole interaction, as expected for very polar species. Dipole-allowed transitions were thus found to be largely dominated by the high partial waves ($l > 4$) with only a small contribution from the FN T-matrices. In contrast, the Born completion for the quadrupole and induced-dipole interactions was found to be negligible: high partial waves were found to increase cross-sections for $\Delta J = 0, 2$ by less than 2 per cent. This clearly shows that cross-sections for dipole forbidden transitions converge rapidly with respect to the partial wave expansion, as observed in the case of molecular ions (e.g. Faure & Tennyson 2001). As a result, only the Born-closure approximation for the dipole interaction was implemented in the computation of the integral rotational cross-sections.

In Fig. 2, we compare our integral cross-sections with those of Jain & Norcross (1985) and Saha et al. (1981). Excellent agreement is observed down to 0.01 eV. At lower energy, we adopted the extrapolation formula of Rabadán, Sarpal & Tennyson (1998) (equation 1 of their paper) which was calibrated using the rotational close-coupling results of Saha et al. (1981). This procedure obviously introduces uncertainties in the rate calculation at

Table 1. Coefficients a_i of the polynomial fit, equation (4), to the rotational de-excitation rate coefficients of HCN. These coefficients are only valid in the temperature range 5–2000 K. $E_{\rm up}$ (K) are the upper level energies.

Transition	$E_{\rm up}$ (K)	a_0	a_1	a_2	a_3	a_4
(1–0)	4.3	−7.543	10.018	−17.974	14.328	−4.169
(2–0)	12.8	−10.923	22.212	−52.611	60.265	−26.660
(2–1)	12.8	−7.552	10.772	−21.515	19.858	−7.067
(3–0)	25.5	−13.297	30.136	−71.602	79.988	−34.340
(3–1)	25.5	−10.830	22.286	−52.461	59.201	−25.830
(3–2)	25.5	−7.589	11.377	−24.257	24.067	−9.239
(4–0)	42.5	−15.647	35.452	−84.761	94.380	−40.338
(4–1)	42.5	−13.222	30.599	−73.095	81.660	−35.036
(4–2)	42.5	−10.827	22.664	−53.590	60.351	−26.259
(4–3)	42.5	−7.633	11.910	−26.550	27.495	−10.976
(5–0)	63.8	−17.755	36.842	−88.707	99.539	−42.965
(5–1)	63.8	−15.718	37.455	−91.762	104.331	−45.407
(5–2)	63.8	−13.277	31.655	−76.702	86.569	−37.456
(5–3)	63.8	−10.815	22.782	−53.882	60.382	−26.134
(5–4)	63.8	−7.677	12.402	−28.613	30.532	−12.492
(6–0)	89.3	−17.947	22.002	−49.290	54.613	−24.371
(6–1)	89.3	−18.379	44.219	−114.389	136.990	−62.411
(6–2)	89.3	−16.049	41.262	−105.105	123.812	−55.550
(6–3)	89.3	−13.426	33.410	−82.796	95.273	−41.916
(6–4)	89.3	−10.888	23.601	−56.532	63.817	−27.757
(6–5)	89.3	−7.737	13.016	−31.039	34.097	−14.297
(7–0)	119.1	−17.477	2.037	2.640	−10.257	8.971
(7–1)	119.1	−19.755	39.818	−106.846	130.991	−59.153
(7–2)	119.1	−20.167	61.606	−172.992	219.967	−103.973
(7–3)	119.1	−17.003	50.704	−137.567	170.812	−79.770
(7–4)	119.1	−13.717	36.432	−93.345	110.640	−49.901
(7–5)	119.1	−10.947	24.277	−58.843	66.970	−29.308
(7–6)	119.1	−7.791	13.571	−33.249	37.364	−15.963
(8–0)	153.1	−9.087	−41.736	42.984	14.247	−28.504
(8–1)	153.1	−14.491	−23.527	84.511	−119.423	58.957
(8–2)	153.1	−16.613	11.279	−11.836	−2.489	6.619
(8–3)	153.1	−17.542	36.928	−88.046	95.525	−39.360
(8–4)	153.1	−18.534	64.949	−184.148	234.228	−109.912
(8–5)	153.1	−14.334	42.448	−114.006	140.539	−65.328
(8–6)	153.1	−11.068	25.526	−63.164	73.166	−32.507
(8–7)	153.1	−7.823	13.903	−34.635	39.376	−16.952

Table 2. Coefficients a_i of the polynomial fit, equation (4), to the rotational de-excitation rate coefficients of DCN. These coefficients are only valid in the temperature range 5–2000 K. $E_{\rm up}$ (K) are the upper level energies.

Transition	$E_{\rm up}$ (K)	a_0	a_1	a_2	a_3	a_4
(1–0)	3.5	−7.513	9.737	−16.754	12.437	−3.174
(2–0)	10.4	−10.931	22.292	−52.959	60.944	−27.038
(2–1)	10.4	−7.527	10.532	−20.385	18.095	−6.144
(3–0)	20.9	−13.275	29.938	−71.022	79.434	−34.150
(3–1)	20.9	−10.799	22.009	−51.638	58.299	−25.449
(3–2)	20.9	−7.561	11.088	−22.909	21.979	−8.157
(4–0)	34.8	−15.559	34.612	−81.872	90.381	−38.336
(4–1)	34.8	−13.189	30.289	−72.067	80.410	−34.476
(4–2)	34.8	−10.794	22.357	−52.623	59.213	−25.753
(4–3)	34.8	−7.592	11.502	−24.778	24.819	−9.611
(5–0)	52.1	−17.594	35.278	−83.187	91.562	−38.855
(5–1)	52.1	−15.554	35.865	−86.214	96.384	−41.332
(5–2)	52.1	−13.199	30.907	−74.137	83.071	−35.733
(5–3)	52.1	−10.807	22.701	−53.656	60.318	−26.194
(5–4)	52.1	−7.643	12.076	−27.155	28.395	−11.451
(6–0)	73.0	−17.202	14.785	−24.098	17.750	−5.212
(6–1)	73.0	−17.737	38.047	−92.971	105.803	−46.244
(6–2)	73.0	−15.705	37.912	−93.299	106.476	−46.487
(6–3)	73.0	−13.236	31.583	−76.490	86.276	−37.307
(6–4)	73.0	−10.843	23.178	−55.163	62.141	−27.005
(6–5)	73.0	−7.677	12.439	−28.711	30.698	−12.601
(7–0)	97.3	−16.289	−7.875	30.337	−38.294	15.702
(7–1)	97.3	−18.107	24.976	−59.631	69.686	−32.154
(7–2)	97.3	−18.405	45.121	−117.556	141.673	−64.869
(7–3)	97.3	−16.011	41.257	−105.090	123.775	−55.517
(7–4)	97.3	−13.372	33.096	−81.743	93.795	−41.171
(7–5)	97.3	−10.838	23.256	−55.432	62.368	−27.064
(7–6)	97.3	−7.728	12.953	−30.725	33.628	−14.069
(8–0)	125.1	−9.469	−41.064	53.519	−24.563	5.360
(8–1)	125.1	−17.037	−1.195	15.814	−33.284	23.214
(8–2)	125.1	−19.699	39.962	−107.384	131.888	−59.701
(8–3)	125.1	−19.905	59.603	−166.518	211.269	−99.909
(8–4)	125.1	−16.738	48.424	−129.770	159.575	−74.013
(8–5)	125.1	−13.600	35.446	−89.911	105.637	−47.303
(8–6)	125.1	−10.913	24.049	−58.131	66.107	−28.940
(8–7)	125.1	−7.765	13.337	−32.316	36.014	−15.296

temperatures below about 100 K, in addition to closed-channel effects which are completely ignored in the present treatment. Hence, rate coefficients below 100 K are expected to be less accurate than at higher temperatures.

A large-shape resonance can be observed in Fig. 2 at about 2.8 eV. It is particularly strong for transitions with small cross-sections, that is, those with $\Delta J > 2$. This resonance (of $^2\Pi$ symmetry) has also been observed experimentally, as discussed in Varambhia & Tennyson (2007). For HNC, it appears at a slightly lower position of 2.5 eV. It is to be noted that the cross-sections for $\Delta J = 1$ are much larger than that for the other transitions due to the dominance of the long-range dipole interaction for very polar molecules.

We finally note that, to our knowledge, there are no data (theoretical or experimental) on the rotational excitation of DCN, HNC and DNC available in the literature.

3.2 Rotational rates

As HCN and HNC (hence DCN and DNC) have their first electronic excitation thresholds at 6.63 and 6.20 eV, respectively, the rotational excitation cross-sections were computed in the range 0.01–6.2 eV and extrapolated down to rotational thresholds (see Section 3.1). Assuming that the electron velocity distribution is Maxwellian, rate coefficients were obtained for temperatures in the range 5–6000 K and for transitions among all levels up to $J = 8$. De-excitation rates were calculated using the detailed balance relation. For later use in modelling, the temperature dependence of the downward transition rates $k(T)$, in units of cm^3 s^{-1}, was fitted to the analytic form (Faure et al. 2004a):

$$\log_{10} k(T) = \sum_{i=0}^{N} a_i x^i, \tag{4}$$

where $x = 1/T^{1/6}$, $N = 4$ and T is restricted to the range 5–2000 K in order to achieve a fitting accuracy of a few per cent. The coefficients $\{a_i\}$, in units such that k is in cm^3 s^{-1}, obtained from the fitting procedure are given in Tables 1, 2, 3 and 4 for HCN, DCN, HNC and DNC, respectively. Fitting coefficients for temperatures above 2000 K and $J > 8$ can be obtained on request from the authors.

Excitation rates are presented in Fig. 3 for HCN and DCN. The small differences with the results of Saha et al. (1981) reflect the sensitivity of low-temperature rates to the near-threshold cross-sections. It can also be noted that the smaller rotational thresholds of DCN (with respect to HCN) lead to a significant but

Table 3. Coefficients a_i of the polynomial fit, equation (4), to the rotational de-excitation rate coefficients of HNC. These coefficients are only valid in the temperature range 5–2000 K. E_{up} (K) are the upper level energies.

Transition	E_{up} (K)	a_0	a_1	a_2	a_3	a_4
(1–0)	4.4	−7.403	8.926	−14.801	10.563	−2.590
(2–0)	13.1	−9.639	14.074	−35.391	44.128	−21.007
(2–1)	13.1	−7.423	9.788	−18.744	16.659	−5.761
(3–0)	26.1	−12.814	28.897	−74.598	89.274	−40.332
(3–1)	26.1	−9.592	14.548	−36.465	44.710	−21.001
(3–2)	26.1	−7.455	10.360	−21.423	20.817	−7.926
(4–0)	43.5	−15.927	39.571	−100.775	117.735	−52.025
(4–1)	43.5	−12.763	29.537	−76.487	91.297	−41.134
(4–2)	43.5	−9.578	14.777	−36.902	44.619	−20.689
(4–3)	43.5	−7.521	11.100	−24.432	25.262	−10.173
(5–0)	65.3	−15.764	21.053	−41.693	38.333	−13.813
(5–1)	65.3	−16.129	42.754	−111.610	133.075	−59.844
(5–2)	65.3	−12.209	24.827	−61.026	71.672	−32.590
(5–3)	65.3	−9.621	15.387	−38.753	46.790	−21.638
(5–4)	65.3	−7.583	11.785	−27.233	29.445	−12.313
(6–0)	91.4	−15.158	1.477	7.836	−15.293	7.402
(6–1)	91.4	−16.923	33.431	−84.174	99.707	−45.347
(6–2)	91.4	−16.830	49.989	−136.387	168.824	−78.263
(6–3)	91.4	−13.108	33.596	−90.122	110.323	−50.739
(6–4)	91.4	−9.107	10.635	−23.005	26.473	−12.585
(6–5)	91.4	−7.668	12.643	−30.602	34.339	−14.756
(7–0)	121.8	−9.723	−58.673	181.107	−236.439	111.453
(7–1)	121.8	−12.497	−22.208	88.515	−132.742	68.301
(7–2)	121.8	−17.644	39.253	−96.958	104.695	−39.340
(7–3)	121.8	−18.318	64.133	−183.445	234.541	−110.659
(7–4)	121.8	−13.698	39.371	−109.796	138.629	−65.302
(7–5)	121.8	−9.814	17.433	−45.443	55.767	−26.026
(7–6)	121.8	−7.686	12.855	−31.518	35.688	−15.428
(8–0)	156.6	−12.532	−8.671	−48.477	123.185	−76.018
(8–1)	156.6	−9.784	−56.529	173.568	−225.735	106.060
(8–2)	156.6	−12.407	−22.181	87.726	−131.074	67.259
(8–3)	156.6	−14.860	14.808	−20.242	5.667	3.941
(8–4)	156.6	−17.161	50.763	−126.624	131.935	−45.525
(8–5)	156.6	−14.757	49.398	−143.428	186.181	−89.164
(8–6)	156.6	−10.025	19.503	−52.460	65.752	−31.138
(8–7)	156.6	−7.546	2.952	7.712	−20.936	12.334

Table 4. Coefficients a_i of the polynomial fit, equation (4), to the rotational de-excitation rate coefficients of DNC. These coefficients are only valid in the temperature range 5–2000 K. E_{up} (K) are the upper level energies.

Transition	E_{up} (K)	a_0	a_1	a_2	a_3	a_4
(1–0)	3.7	−7.384	8.764	−13.998	9.270	−1.898
(2–0)	11.0	−9.621	13.929	−35.013	43.803	−20.891
(2–1)	11.0	−7.388	9.471	−17.374	14.561	−4.671
(3–0)	22.0	−12.764	28.480	−73.414	87.992	−39.825
(3–1)	22.0	−9.554	14.223	−35.527	43.683	−20.576
(3–2)	22.0	−7.415	9.987	−19.843	18.427	−6.694
(4–0)	36.6	−15.858	38.929	−98.621	114.823	−50.591
(4–1)	36.6	−12.724	29.182	−75.374	89.958	−40.533
(4–2)	36.6	−9.556	14.614	−36.544	44.501	−20.775
(4–3)	36.6	−7.475	10.691	−22.757	22.803	−8.942
(5–0)	54.9	−15.543	18.882	−34.000	27.004	−7.873
(5–1)	54.9	−15.904	40.627	−104.370	122.762	−54.559
(5–2)	54.9	−12.752	29.932	−77.731	92.857	−41.854
(5–3)	54.9	−9.558	14.818	−36.983	44.601	−20.644
(5–4)	54.9	−7.533	11.316	−25.280	26.537	−10.839
(6–0)	76.9	−13.939	−10.066	47.036	−71.217	35.657
(6–1)	76.9	−15.950	24.200	−52.614	54.255	−22.087
(6–2)	76.9	−16.211	44.121	−116.306	139.844	−63.333
(6–3)	76.9	−12.874	31.372	−82.537	99.488	−45.176
(6–4)	76.9	−9.596	15.308	−38.466	46.324	−21.378
(6–5)	76.9	−7.577	11.788	−27.254	29.476	−12.326
(7–0)	102.5	−12.645	−31.579	91.009	−110.232	49.377
(7–1)	102.5	−15.491	5.896	−6.381	3.094	−0.486
(7–2)	102.5	−17.326	37.781	−98.624	119.852	−55.263
(7–3)	102.5	−16.959	51.549	−141.660	176.358	−82.102
(7–4)	102.5	−13.109	33.807	−90.846	111.375	−51.288
(7–5)	102.5	−9.671	16.091	−40.984	49.613	−22.945
(7–6)	102.5	−7.628	12.320	−29.380	32.606	−13.908
(8–0)	131.8	−13.106	−2.647	−70.842	157.263	−94.056
(8–1)	131.8	−9.600	−58.397	180.148	−235.148	110.842
(8–2)	131.8	−12.423	−22.254	88.666	−132.965	68.413
(8–3)	131.8	−17.403	37.141	−88.825	91.193	−31.327
(8–4)	131.8	−18.257	63.816	−182.467	233.321	−110.159
(8–5)	131.8	−13.595	38.537	−106.951	134.530	−63.196
(8–6)	131.8	−9.779	17.182	−44.598	54.590	−25.434
(8–7)	131.8	−7.665	12.717	−31.059	35.143	−15.217

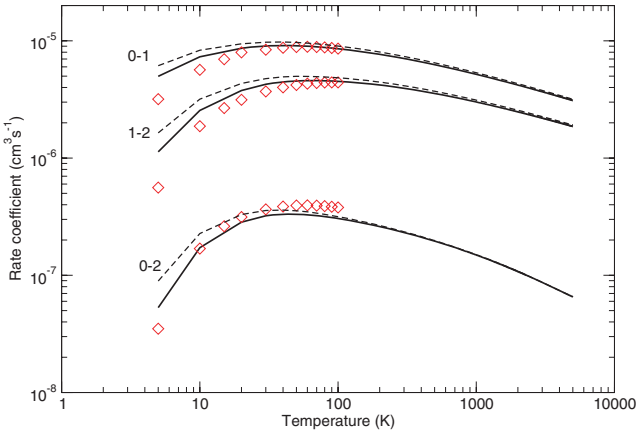

Figure 3. Rate coefficients for rotational excitation of HCN and DCN by electron-impact as a function of temperature. The lozenges denote the HCN calculations of Saha et al. (1981) while the solid and dashed lines give the present results for HCN and DCN, respectively.

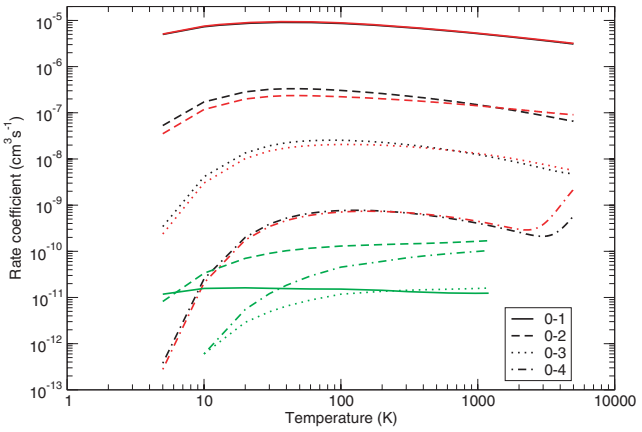

Figure 4. Rate coefficients for rotational excitation of HCN and HNC as a function of temperature. The black and red lines denote the present results for electron-impact excitation of HCN and HNC, respectively. The green line gives the results of Green & Thaddeus (1974) and Green (unpublished data) for the rotational excitation of HCN by He atoms.

moderate increase in rates below 100 K. As a result, rates for other isotopologues such as H^{13}CN and H^{15}NC are expected to be very similar to those of HCN and HNC, respectively, since the rotational thresholds are only slightly different.

In Fig. 4, electron-impact rate coefficients for HCN and HNC are presented along with rates for excitation of HCN by He atoms. It is firstly observed that HCN and HNC have similar rates, with typical differences less than 50 per cent for the plotted transitions. Note that the dipolar $0 \rightarrow 1$ curves are almost superposed in the whole temperature range. This reflects the dominance of the dipole interaction. Differences larger than a factor of 2 were, however, found for the smallest rates, that is, those corresponding to transitions with $\Delta J > 2$. Secondly, rate coefficients for excitation by He atoms are much smaller than electron-impact rates. In particular, the He–HCN rate for the transition $0 \rightarrow 1$ is about six orders of magnitude smaller than the e–HCN rate. Furthermore, the propensity rules are very different, with even ΔJ strongly favoured over odd ΔJ in the case of He. This propensity reflects an interference effect related to the even anisotropy of the He–HCN potential energy surface (e.g. McCurdy & Miller 1977). As a result, the difference between e–HCN and He–HCN rates is much larger for dipole-allowed transitions than for other transitions. For instance, the He–HCN rate coefficient for the transition $0 \rightarrow 4$ at 1000 K is only a factor of 4 smaller than the electron-impact rate.

These large differences between He–HCN and e–HCN rotational rates, both in terms of magnitude and propensity rules, suggest that the modelling of HCN excitation in astrophysical environments must be very sensitive to the relative abundance of electrons and neutrals.

3.3 Hyperfine rates

Hyperfine rate coefficients were computed from the pure rotational rates using the formalism proposed by Neufeld & Green (1994),

Table 5. Hyperfine de-excitation rates in cm^3 s^{-1} for HCN, where necessary powers of 10 are given in parentheses.

J	F	J'	F'	10 K	100 K	1000 K
1	0	0	1	0.373(−5)	0.297(−5)	0.173(−5)
1	1	0	1	0.373(−5)	0.297(−5)	0.173(−5)
1	1	1	0	0.0	0.0	0.0
1	2	0	1	0.373(−5)	0.297(−5)	0.173(−5)
1	2	1	0	0.492(−7)	0.277(−7)	0.121(−7)
1	2	1	1	0.111(−6)	0.624(−7)	0.272(−7)
2	1	0	1	0.123(−6)	0.693(−7)	0.302(−7)
2	1	1	0	0.199(−5)	0.164(−5)	0.101(−5)
2	1	1	1	0.149(−5)	0.123(−5)	0.757(−6)
2	1	1	2	0.110(−6)	0.887(−7)	0.533(−7)
2	2	0	1	0.123(−6)	0.693(−7)	0.302(−7)
2	2	1	0	0.0	0.0	0.0
2	2	1	1	0.269(−5)	0.221(−5)	0.136(−5)
2	2	1	2	0.902(−6)	0.740(−6)	0.456(−6)
2	2	2	1	0.615(−7)	0.346(−7)	0.151(−7)
2	3	0	1	0.123(−6)	0.693(−7)	0.302(−7)
2	3	1	0	0.259(−8)	0.165(−8)	0.683(−9)
2	3	1	1	0.518(−8)	0.331(−8)	0.137(−8)
2	3	1	2	0.358(−5)	0.295(−5)	0.182(−5)
2	3	2	1	0.524(−8)	0.297(−8)	0.128(−8)
2	3	2	2	0.504(−7)	0.284(−7)	0.124(−7)
3	2	0	1	0.756(−8)	0.467(−8)	0.182(−8)
3	2	1	0	0.652(−7)	0.398(−7)	0.179(−7)
3	2	1	1	0.652(−7)	0.398(−7)	0.179(−7)
3	2	1	2	0.961(−8)	0.591(−8)	0.264(−8)
3	2	2	1	0.277(−5)	0.232(−5)	0.150(−5)
3	2	2	2	0.516(−6)	0.433(−6)	0.279(−6)
3	2	2	3	0.157(−7)	0.130(−7)	0.826(−8)
3	3	0	1	0.756(−8)	0.467(−8)	0.182(−8)
3	3	1	0	0.0	0.0	0.0
3	3	1	1	0.932(−7)	0.570(−7)	0.256(−7)
3	3	1	2	0.468(−7)	0.286(−7)	0.129(−7)
3	3	2	1	0.260(−8)	0.169(−8)	0.732(−9)
3	3	2	2	0.293(−5)	0.246(−5)	0.159(−5)
3	3	2	3	0.369(−6)	0.310(−6)	0.200(−6)
3	3	3	2	0.353(−7)	0.199(−7)	0.866(−8)
3	4	0	1	0.756(−8)	0.467(−8)	0.182(−8)
3	4	1	0	0.777(−10)	0.554(−10)	0.207(−10)
3	4	1	1	0.146(−9)	0.104(−9)	0.388(−10)
3	4	1	2	0.140(−6)	0.854(−7)	0.384(−7)
3	4	2	1	0.288(−9)	0.188(−9)	0.813(−10)
3	4	2	2	0.240(−8)	0.157(−8)	0.677(−9)
3	4	2	3	0.330(−5)	0.277(−5)	0.179(−5)
3	4	3	2	0.134(−8)	0.759(−9)	0.329(−9)
3	4	3	3	0.286(−7)	0.161(−7)	0.702(−8)

Table 6. Hyperfine de-excitation rates in $cm^3\ s^{-1}$ for DCN, where necessary powers of 10 are given in parentheses.

J	F	J'	F'	10 K	100 K	1000 K
1	0	0	1	0.392(−5)	0.311(−5)	0.179(−5)
1	1	0	1	0.392(−5)	0.311(−5)	0.179(−5)
1	1	1	0	0.0	0.0	0.0
1	2	0	1	0.392(−5)	0.311(−5)	0.179(−5)
1	2	1	0	0.516(−7)	0.281(−7)	0.121(−7)
1	2	1	1	0.116(−6)	0.632(−7)	0.273(−7)
2	1	0	1	0.129(−6)	0.702(−7)	0.303(−7)
2	1	1	0	0.212(−5)	0.172(−5)	0.105(−5)
2	1	1	1	0.159(−5)	0.129(−5)	0.786(−6)
2	1	1	2	0.117(−6)	0.933(−7)	0.553(−7)
2	2	0	1	0.129(−6)	0.702(−7)	0.303(−7)
2	2	1	0	0.0	0.0	0.0
2	2	1	1	0.286(−5)	0.233(−5)	0.142(−5)
2	2	1	2	0.960(−6)	0.780(−6)	0.474(−6)
2	2	2	1	0.645(−7)	0.351(−7)	0.152(−7)
2	3	0	1	0.129(−6)	0.702(−7)	0.303(−7)
2	3	1	0	0.277(−8)	0.170(−8)	0.689(−9)
2	3	1	1	0.554(−8)	0.341(−8)	0.138(−8)
2	3	1	2	0.381(−5)	0.310(−5)	0.189(−5)
2	3	2	1	0.550(−8)	0.301(−8)	0.129(−8)
2	3	2	2	0.529(−7)	0.288(−7)	0.124(−7)
3	2	0	1	0.798(−8)	0.478(−8)	0.183(−8)
3	2	1	0	0.685(−7)	0.406(−7)	0.180(−7)
3	2	1	1	0.685(−7)	0.406(−7)	0.180(−7)
3	2	1	2	0.101(−7)	0.602(−8)	0.266(−8)
3	2	2	1	0.298(−5)	0.247(−5)	0.156(−5)
3	2	2	2	0.556(−6)	0.459(−6)	0.290(−6)
3	2	2	3	0.169(−7)	0.138(−7)	0.857(−8)
3	3	0	1	0.798(−8)	0.478(−8)	0.183(−8)
3	3	1	0	0.0	0.0	0.0
3	3	1	1	0.979(−7)	0.581(−7)	0.258(−7)
3	3	1	2	0.491(−7)	0.291(−7)	0.129(−7)
3	3	2	1	0.280(−8)	0.175(−8)	0.739(−9)
3	3	2	2	0.315(−5)	0.261(−5)	0.165(−5)
3	3	2	3	0.397(−6)	0.328(−6)	0.207(−6)
3	3	3	2	0.370(−7)	0.202(−7)	0.869(−8)
3	4	0	1	0.798(−8)	0.478(−8)	0.183(−8)
3	4	1	0	0.825(−10)	0.574(−10)	0.209(−10)
3	4	1	1	0.155(−9)	0.108(−9)	0.392(−10)
3	4	1	2	0.147(−6)	0.870(−7)	0.386(−7)
3	4	2	1	0.312(−9)	0.195(−9)	0.821(−10)
3	4	2	2	0.260(−8)	0.162(−8)	0.684(−9)
3	4	2	3	0.355(−5)	0.294(−5)	0.186(−5)
3	4	3	2	0.141(−8)	0.769(−9)	0.330(−9)
3	4	3	3	0.300(−7)	0.163(−7)	0.705(−8)

Table 7. Hyperfine de-excitation rates in $cm^3\ s^{-1}$ for HNC, where necessary powers of 10 are given in parentheses.

J	F	J'	F'	10 K	100 K	1000 K
1	0	0	1	0.388(−5)	0.307(−5)	0.177(−5)
1	1	0	1	0.388(−5)	0.307(−5)	0.177(−5)
1	1	1	0	0.0	0.0	0.0
1	2	0	1	0.388(−5)	0.307(−5)	0.177(−5)
1	2	1	0	0.347(−7)	0.203(−7)	0.115(−7)
1	2	1	1	0.780(−7)	0.456(−7)	0.259(−7)
2	1	0	1	0.867(−7)	0.507(−7)	0.288(−7)
2	1	1	0	0.205(−5)	0.167(−5)	0.103(−5)
2	1	1	1	0.154(−5)	0.126(−5)	0.770(−6)
2	1	1	2	0.111(−6)	0.893(−7)	0.543(−7)
2	2	0	1	0.867(−7)	0.507(−7)	0.288(−7)
2	2	1	0	0.0	0.0	0.0
2	2	1	1	0.277(−5)	0.226(−5)	0.139(−5)
2	2	1	2	0.928(−6)	0.757(−6)	0.464(−6)
2	2	2	1	0.434(−7)	0.254(−7)	0.144(−7)
2	3	0	1	0.867(−7)	0.507(−7)	0.288(−7)
2	3	1	0	0.199(−8)	0.134(−8)	0.719(−9)
2	3	1	1	0.398(−8)	0.267(−8)	0.144(−8)
2	3	1	2	0.369(−5)	0.302(−5)	0.185(−5)
2	3	2	1	0.373(−8)	0.220(−8)	0.123(−8)
2	3	2	2	0.356(−7)	0.208(−7)	0.118(−7)
3	2	0	1	0.586(−8)	0.381(−8)	0.193(−8)
3	2	1	0	0.459(−7)	0.293(−7)	0.172(−7)
3	2	1	1	0.459(−7)	0.293(−7)	0.172(−7)
3	2	1	2	0.683(−8)	0.438(−8)	0.254(−8)
3	2	2	1	0.284(−5)	0.237(−5)	0.152(−5)
3	2	2	2	0.528(−6)	0.440(−6)	0.282(−6)
3	2	2	3	0.158(−7)	0.131(−7)	0.836(−8)
3	3	0	1	0.586(−8)	0.381(−8)	0.193(−8)
3	3	1	0	0.0	0.0	0.0
3	3	1	1	0.657(−7)	0.419(−7)	0.246(−7)
3	3	1	2	0.330(−7)	0.210(−7)	0.123(−7)
3	3	2	1	0.198(−8)	0.136(−8)	0.767(−9)
3	3	2	2	0.300(−5)	0.250(−5)	0.161(−5)
3	3	2	3	0.378(−6)	0.315(−6)	0.202(−6)
3	3	3	2	0.249(−7)	0.146(−7)	0.827(−8)
3	4	0	1	0.586(−8)	0.381(−8)	0.193(−8)
3	4	1	0	0.699(−10)	0.522(−10)	0.229(−10)
3	4	1	1	0.131(−9)	0.978(−10)	0.429(−10)
3	4	1	2	0.985(−7)	0.628(−7)	0.368(−7)
3	4	2	1	0.220(−9)	0.151(−9)	0.852(−10)
3	4	2	2	0.184(−8)	0.126(−8)	0.710(−9)
3	4	2	3	0.338(−5)	0.282(−5)	0.181(−5)
3	4	3	2	0.952(−9)	0.560(−9)	0.315(−9)
3	4	3	3	0.202(−7)	0.118(−7)	0.670(−8)

as explained in Section. 2.3. Sample results are presented in Tables 5, 6, 7 and 8 for HCN, DCN, HNC and DNC, respectively. Additional hyperfine data at different temperatures and for higher rotational levels can be obtained on request from the authors. The relative propensities predicted by our calculations at 20 K for a few hyperfine transitions induced by electron-impact are given in Table 9 and are compared to He−HCN results. First, it may be seen that the present implementation of the method of Neufeld & Green (1994), that is based on downward fundamental rates, gives a reasonable agreement with the accurate close-coupling results of Monteiro & Stutzki (1986) for He–HCN. Errors on rate values were thus found to range between typically 10 and 50 per cent, suggesting that the IOS scaling of rotational rates provides a rather good description of hyperfine rates. Secondly, it is found that the well-known propensity rule $\Delta J = \Delta F$ is stronger for e–HCN than for He–HCN. This propensity rule was derived and confirmed experimentally by Alexander & Dagdigian (1985) for the case of atom–molecule collisions. As discussed by these authors, the $\Delta J = \Delta F$ propensity is independent of dynamics and follows properties of Wigner-6j symbols (see Section 2.3). It is thus expected to become increasingly strong as J and J' increase, as indeed observed in Tables 5–8. The fact that it is stronger for electrons than for He atoms is simply due to the smallness of electron-impact rates for transitions with $\Delta J > 2$.

It should be noted that in the case of He–N_2H^+ collisions, Daniel et al. (2005) have found that the $\Delta J = \Delta F$ propensity does not always apply at low energy, owing to the presence of closed-channel resonances. The importance of such effects for electron–molecule collisions is, however, unclear and would deserve further studies.

Table 8. Hyperfine de-excitation rates in $cm^3\ s^{-1}$ for DNC, where necessary powers of 10 are given in parentheses.

J	F	J'	F'	10 K	100 K	1000 K
1	0	0	1	0.408(−5)	0.321(−5)	0.183(−5)
1	1	0	1	0.408(−5)	0.321(−5)	0.183(−5)
1	1	1	0	0.0	0.0	0.0
1	2	0	1	0.408(−5)	0.321(−5)	0.183(−5)
1	2	1	0	0.360(−7)	0.205(−7)	0.115(−7)
1	2	1	1	0.811(−7)	0.462(−7)	0.259(−7)
2	1	0	1	0.901(−7)	0.513(−7)	0.288(−7)
2	1	1	0	0.218(−5)	0.176(−5)	0.106(−5)
2	1	1	1	0.163(−5)	0.132(−5)	0.799(−6)
2	1	1	2	0.118(−6)	0.939(−7)	0.563(−7)
2	2	0	1	0.901(−7)	0.513(−7)	0.288(−7)
2	2	1	0	0.0	0.0	0.0
2	2	1	1	0.294(−5)	0.238(−5)	0.144(−5)
2	2	1	2	0.986(−6)	0.797(−6)	0.481(−6)
2	2	2	1	0.450(−7)	0.256(−7)	0.144(−7)
2	3	0	1	0.901(−7)	0.513(−7)	0.288(−7)
2	3	1	0	0.211(−8)	0.137(−8)	0.726(−9)
2	3	1	1	0.421(−8)	0.274(−8)	0.145(−8)
2	3	1	2	0.392(−5)	0.318(−5)	0.192(−5)
2	3	2	1	0.388(−8)	0.223(−8)	0.123(−8)
2	3	2	2	0.370(−7)	0.211(−7)	0.118(−7)
3	2	0	1	0.614(−8)	0.388(−8)	0.194(−8)
3	2	1	0	0.479(−7)	0.297(−7)	0.172(−7)
3	2	1	1	0.479(−7)	0.297(−7)	0.172(−7)
3	2	1	2	0.713(−8)	0.445(−8)	0.254(−8)
3	2	2	1	0.304(−5)	0.251(−5)	0.158(−5)
3	2	2	2	0.566(−6)	0.467(−6)	0.293(−6)
3	2	2	3	0.170(−7)	0.139(−7)	0.868(−8)
3	3	0	1	0.614(−8)	0.388(−8)	0.194(−8)
3	3	1	0	0.0	0.0	0.0
3	3	1	1	0.686(−7)	0.425(−7)	0.246(−7)
3	3	1	2	0.344(−7)	0.213(−7)	0.123(−7)
3	3	2	1	0.212(−8)	0.140(−8)	0.774(−9)
3	3	2	2	0.321(−5)	0.265(−5)	0.167(−5)
3	3	2	3	0.404(−6)	0.334(−6)	0.210(−6)
3	3	3	2	0.259(−7)	0.147(−7)	0.827(−8)
3	4	0	1	0.614(−8)	0.388(−8)	0.194(−8)
3	4	1	0	0.737(−10)	0.536(−10)	0.231(−10)
3	4	1	1	0.138(−9)	0.100(−9)	0.432(−10)
3	4	1	2	0.103(−6)	0.636(−7)	0.368(−7)
3	4	2	1	0.235(−9)	0.156(−9)	0.860(−10)
3	4	2	2	0.196(−8)	0.130(−8)	0.717(−9)
3	4	2	3	0.362(−5)	0.299(−5)	0.188(−5)
3	4	3	2	0.990(−9)	0.567(−9)	0.315(−9)
3	4	3	3	0.210(−7)	0.120(−7)	0.670(−8)

It can be noted in Tables 5–8 that in addition to the $\Delta J = \Delta F$ propensity rule, there is a rigorous selection rule at the IOS level: the $(J, F = J) \rightarrow (J' = 1, F' = 0)$ transitions are strictly forbidden, following properties of Wigner-6*j* symbols. Monteiro & Stutzki (1986) have shown that for He–HCN this selection rule becomes only a propensity rule at the close-coupling level.

Finally, we note that the influence of collisional processes on HCN hyperfine anomalies is still a matter of debate in the literature (e.g. González-Alfonso & Cernicharo 1993; Turner 2001; Daniel, Cernicharo & Dubernet 2006). Future radiative transfer studies including the present hyperfine rates will thus help to further assess the role of collision-induced transitions between HCN hyperfine levels. In this context, it is important to remember that H_2–HCN collisional rates are currently obtained by scaling He–HCN rates by the reduced mass ratio. While for para-$H_2(J = 0)$ this assumption is probably qualitatively correct, rates for $H_2(J \neq 0)$ might be significantly different, as found, for example, in the case of H_2–H_2O (Faure et al. 2007, and references therein). Furthermore, it is worth stressing that rates for excitation of HCN by H atoms and H_2O molecules are completely unknown.

Table 9. Relative propensities for hyperfine collisional rates as a percentage of the total rates for $T = 20$ K. Present = rates calculated here; He (CC) = close-coupling He–HCN results of Monteiro & Stutzki (1986); He (IOS) = IOS scaling for He–HCN.

J	F	J'	F'	Present	He (CC)	He (IOS)
1	1	2	1	24.9	21.4	19.2
		2	2	74.9	59.7	65.4
		2	3	0.2	18.9	15.4
1	1	3	2	33.3	30.0	26.3
		3	3	66.6	61.3	60.5
		3	4	0.1	8.8	13.2
2	2	3	2	11.2	17.0	16.6
		3	3	88.7	69.8	75.8
		3	4	0.1	13.3	7.7

4 CONCLUSIONS

We have calculated electron-impact rotational and hyperfine (de)excitation rates for isotopologues of HCN and HNC. These calculations are based on the molecular R-matrix method combined with the (threshold-corrected) ANR approximation. Our results show that such collisions are essentially dominated by dipolar transitions, owing to the large dipole moments of the considered species. However, short-range effects are important and were included via R-matrix wavefunctions as corrections to the Born approximation. Dipole forbidden transitions have thus appreciable rates which cannot be neglected in any detailed population models of isotopologues of HCN and HNC. In particular, we have shown that electron-impact rates are crucial for modelling environments where the electron fraction is larger than 10^{-6}. In this context, we note the recent suggestion by Jimenez-Serra et al. (2006) to use rotational emissions of HCO^+, HCN and HNC to probe electron densities in C-type shocks. The present rates should help to investigate in more detail the electron density enhancements expected during the first stages of a C-type shock evolution. Finally, our work might help to understand and to model the observed variable HCN/HNC ratio in comets (Biver et al. 2006, and references therein).

ACKNOWLEDGMENTS

AF acknowledges support by the CNRS national program "Physique et Chimie du Millieu Interstellaire".

REFERENCES

Aalto S., Polatidis A. G., Hutemeister S., Curran S. J., 2002, A&A, 381, 783
Ahrens V., Lewen F., Takano S., Winnewisser G., Urban S., Negirev A. A., Koroliev A. N., 2002, Z. NaturForsch, 57, 669
Alexander M. H., Dagdigian P. J., 1985, J. Chem. Phys., 83, 2191
Bechtel H. A., Steeves A. H., Field R. W., 2006, ApJ, 649, L53–L56
Biver N. et al., 2006, A&A, 449, 1255
Blackman G. L., Brown R. D., Godfrey P. D., Gunn H. I., 1976, Nat, 261, 395

Brunken S., Muller H. S. P., Thorwirth S., Lewen F., Winnewisser G., 2006, J. Mol. Struct., 781, 3
Cernicharo J. et al., 1996, A&A, 315, L201
Chang E. S., Temkin A., 1970, J. Phys. Soc. Jap., 29, 172
Chu S.-I., 1976, ApJ, 206, 640
Corey G. C., McCourt F. R., 1983, J. Phys. Chem., 87, 2723
Crawford O. H., Dalgarno A., 1971, J. Phys. B: At. Mol. Phys., 4, 494
Čurík R., Ziesel J. P., Jones N. C., Field T. A., Field D., 2006, Phys. Rev. Lett., 97, 123202
Daniel F., Dubernet M.-L., Meuwly M., Cernicharo J., Pagani L., 2005, MNRAS, 363, 1083
Daniel F., Cernicharo J., Dubernet M.-L., 2006, ApJ, 648, 461
Dickinson A. S., Phillips T. G., Goldsmith P. F., Percival I. C., Richards D., 1977, A&A, 54, 645
Ebenstein W. L., Muenter J. S., 1984, J. Chem. Phys., 80, 3989
Faure A., Tennyson J., 2001, MNRAS, 325, 443
Faure A., Gorfinkiel J. D., Morgan L. A., Tennyson J., 2002, Comput. Phys. Commun., 144, 224
Faure A., Gorfinkiel J. D., Tennyson J., 2004a, MNRAS, 347, 323
Faure A., Gorfinkiel J. D., Tennyson J., 2004b, J. Phys. B: At. Mol. Opt. Phys., 37, 801
Faure A., Kokoouline V., Greene C. H., Tennyson J., 2006, J. Phys. B: At. Mol. Opt. Phys., 39, 4261
Faure A., Crimier N., Ceccarelli C., Valiron P., Wiesenfeld L., Dubernet M.-L., 2007, A&A, 472, 1029
Gil T. J., Lengsfield B. H., McCurdy C. W., Rescigno T. N., 1994, Phys. Rev. A, 49, 2551
González-Alfonso E., Cernicharo J., 1993, A&A, 279, 506
Gorfinkiel J. D., Tennyson J., 2004, J. Phys. B: At. Mol. Opt. Phys., 37, L343
Green S., unpublished data available at http://data.giss.nasa.gov/mcrates/#hcn
Green S., Thaddeus P., 1974, ApJ, 191, 653L
Guélin M. et al., 2007, A&A, 462, L45
Guilloteau S., Baudry A., 1981, A&A, 97, 213
Itikawa Y., 2000, Theor. Chem. Acc., 105, 123
Izumiura H., Ukita N., Tsuji T., 1995, ApJ, 440, 728
Jain A., Norcross D. W., 1985, Phys. Rev. A, 32, 134
Jimenez-Serra I., Martin-Pintado J., Viti S., Martin S., Rodriguez-Franco A., Faure A., Tennyson J., 2006, ApJ, 650, L135
Korsch H. J., Ernesti A., 1992, J. Phys. B: At. Mol. Opt. Phys., 25, 3565
Lane N. F., 1980, Rev. Mod. Phys., 52, 29
Leurini S. et al., 2006, A&A, 454, L47
Lovell A. J., Kallivayalil N., Schloerb F. P., Combi M. R., Hansen K. C., Gombosi T. I., 2004, ApJ, 613, 615L
Lucas R., Cernicharo J., 1989, A&A, 218, L20
McCurdy C. W., Miller W. H., 1977, J. Chem. Phys., 67, 463
Park Y. S., Kim J., Minh Y. C., 1999, ApJ, 520, 223
Monteiro T. S., Stutzki J., 1986, MNRAS, 221, 33P
Morgan L. A., Tennyson J., Gillan C. J., 1998, Comput. Phys. Commun., 114, 120
Morrison M. A., 1988, Adv. At. Mol. Phys., 24, 51
Neufeld D. A., Green S., 1994, ApJ, 432, 158
Rabadán I., Sarpal B. K., Tennyson J., 1998, MNRAS, 299, 171
Saha S., Ray. S., Bhattacharyya B., Barua A. K., 1981, Phys. Rev. A., 23,6, 2926L
Srivastava S. K., Tanaka H., Chutjian A., 1978, J. Chem. Phys., 69, 1493
Turner B. E., 2001, ApJS, 136, 579
Varambhia H. N., Tennyson J., 2007, J. Phys. B: At. Mol. Opt. Phys., 40, 1211
Varshalovich D. A., Khersonskii V. K., 1977, ApL, 18, 167
Walmsley C. M., Churchwell E., Fitzpatrick E., 1982, ApJ, 258, L75

This paper has been typeset from a TEX/LATEX file prepared by the author.